First-principles Insights Into the Structural, Mechanical, Optical, Magnetic, Electronic, and Dynamical Properties of Hf_2CdN MAX phase Compound

Suraj Timsina, Bibek Dhital[1], Sushil Shrestha, Dipesh Dhital, Ganesh Paudel, Om Shree Rijal, Hari Krishna Neupane*

Amrit Campus, Institute of Science and Technology, Tribhuvan University, Kathmandu, Nepal

Research Article

ISSN: 3059-9504 (online)
DOI: https://doi.org/ 10.3126/ajs.v2i1.87758

Article History

Received: October 02, 2025; Revised: November 05, 2025; Accepted: November 15, 2025; Published: December 25, 2025

Keywords

DFT, dynamical properties, electronic properties, magnetic moment, mechanical stability, optical properties.

***Corresponding author**

Email: hari.neupane@ac.tu.edu.np
Orcid: https://orcid.org/0000-0001-8547-1183

ABSTRACT

The MAX phase compounds possess both ceramic and metallic properties and have attracted great attention from researchers. In this work, we studied the structural, mechanical, optical, magnetic, electronic, and dynamical properties of the Hf_2CdN MAX phase compound using the density functional theory (DFT) method through the Quantum ESPRESSO as a computational tool. The low value of ground-state energy confirms the structural stability of our compound. The calculated elastic constants of Hf_2CdN satisfy Born's stability criteria, indicating that it is mechanically stable. Based on the estimated mechanical parameters, Hf_2CdN exhibits anisotropic behavior, metallic-like bonding, and a brittle nature. The phonon frequency curve shows positive values, confirming that the compound is dynamically stable. From the analysis of band structure and density of states (DOS) plots, it reveals that some energy bands cross the Fermi level, indicating metallic behavior. A high absorption coefficient is observed in the visible and UV regions, suggesting potential applications in optoelectronic devices. The strong reflectivity in the UV region further highlights its suitability for radiation shielding and UV mirror materials. Additionally, the high refractive index in the infrared region suggests possible use in optoelectronic applications. From the partial and total, density of states (PDOS and TDOS) analyses, we confirm that Hf_2CdN is nonmagnetic due to the symmetric distribution of spin-up and spin-down electron states near the Fermi level. Overall, our findings provide fundamental insights into the properties of Hf_2CdN and its potential applications in various technological fields, such as it would be used in the fields of optoelectronic devices, UV radiation detectors, mirror coatings in UV lasers, and thermal imaging coatings.

1. INTRODUCTION

MAX phase compounds have a wide range of applications due to their interesting and unique combination of metallic and ceramic properties [1]. High-temperature coatings, magnetic sensors, and energy storage devices are some of their application areas [2, 3]. In general, MAX phases are denoted by the formula $M_{n+1}AX_n$, where M is an early transition metal, A is a group A element, and X is carbon or nitrogen [4]. Hf_2CdN is a 211-type MAX phase compound, where Hf, Cd, and N correspond to M, A, and X, respectively. The electronic configurations of Hf, Cd, and N are [Xe] $4f^{14}5d^26s^2$, [Kr] $4d^{10}5s^2$, and $1s^22s^22p^3$, respectively. This compound crystallizes in a hexagonal structure with space group $P6_3/mmc$ (No. 194) [5]. In this structure, Hf layers alternate with Cd layers, and N atoms located inside the Hf-centered octahedra form Hf–N bonds. Hadi and co-authors in 2015, investigated the fundamental properties of Mo_2GaC, Nb_2AsC, Nb_2InC, and Ti_2GeC using the plane-wave pseudopotential method [6]. Ali and co-authors studied the physical properties of a new MAX phase compound, Mo_2TiAlC_2, using the density functional theory (DFT) method [7]. Roknuzzaman and co-workers in 2017, explored the first Hf-based 312 MAX phase compound using a first-principles approach [8]. Sultan and co-authors in 2018, examined the physical properties of M_2InC (M = Zr, Hf, Ta) using the DFT approach [9]. In 2019, Hadi and co-authors studied the physical, lattice thermal conductivity, and vibrational properties of Lu_2SnC [10]. The computational prediction of boron-based MAX phases and MXene derivatives is carried out by Miao and co-authors [11]. Using a first-principles approach, Yang and his team in 2022, studied the elastic properties, tensile strength, damage tolerance, and electronic and thermal properties of TM_3AlC_2 (TM = Ti, Zr, and Hf) MAX phase compounds [12]. Belkacem and co-authors in 2022, investigated the stability and efficiency of the new MAX phase compounds M_3GaC_2 (M = Ti or Zr) [13]. Rougab and Gueddouh in 2023, explored the structural stability, elastic anisotropies, and mechanical and thermodynamic properties of Hf_2GeX (X = C, N, and B) using first-principles calculations [14]. Haq and his team in 2024, studied the physical properties of Cr_2PX (X = C and N) MAX phase compounds using a first-principles calculations [15]. Rijal and co-authors in 2025, investigated the physical properties of Ti_2CdC and Ti_2SC MAX phase compounds using the DFT method [16]. From these studies, it can be inferred that MAX phase ompounds have potential applications in thermal barrier coatings, optoelectronic devices, thermal shock-resistant materials, solar heating, and coating technologies. Among the reviewed literature on MAX phase compounds, to the best of our knowledge, the structural, mechanical, magnetic, optical, dynamical, and electronic properties of the Hf_2CdN MAX phase compound have not yet been explored. Therefore, our study is motivated by the need to investigate these properties of Hf_2CdN using first-principles calculations with in Quantum ESPRESSO (QE) as a computational tool [14, 15].

2. METHODOLOGY

The structural, mechanical, dynamical, electronic, magnetic, and optical properties of the Hf_2CdN MAX phase compound were investigated using the density functional theory (DFT) method [17]

implemented in the Quantum ESPRESSO (QE) as a computational tool [18]. All calculations are performed using the Perdew–Burke–Ernzerhof (PBE) functional with ultrasoft pseudopotentials (USPs) [19]. For the structural visualizations and graphical exploration, we have used XCrysDen and XmGrace [20, 21]. The structural parameters of the MAX phase compound are optimized using a plane-wave-based DFT method within the GGA-PBE approximation, where the exchange–correlation functional is treated using ultrasoft pseudopotentials (USPs). A kinetic energy cutoff of 520 eV and a Monkhorst–Pack (MP) [22] k-point mesh of (8 × 8 × 8) for band structure and (16 × 16 × 16) for the density of states (DOS) and partial DOS (PDOS) calculations are used. The lattice constants and atomic positions are fully relaxed until the residual forces are less than 0.01 eV/Å and the total energy converged within 10^{-7} eV. After structural optimization, the bond lengths are determined. Based on the M–X and M–A bond lengths, the nature of atomic bonding (ionic or metallic) is analyzed. The elastic constants C_{ij} are calculated using the stress–strain method within DFT [23]. For the hexagonal crystal system, the five independent elastic constants C_{11}, C_{12}, C_{13}, C_{33}, and C_{44} are computed. The Voigt–Reuss–Hill approximations [24, 25, 26] are employed to derive various mechanical properties, including the bulk modulus (B), shear modulus (G), and Young's modulus (E). To assess ductility or brittleness, Poisson's ratio (ν) and Pugh's ratio (B/G) are calculated. The universal anisotropic index [27] is used to evaluate elastic anisotropy (isotropic or anisotropic nature). Additionally, Kleinman's parameter [28] is computed to characterize the bonding nature in terms of stretching or bending. For the hardness properties, the Vickers hardness is calculated. The highly symmetric points within the Brillouin zone are determined using QE. To confirm dynamical stability, phonon frequency plots are generated along these high-symmetry points, and the nature of the phonon dispersion is analyzed. The electronic structure is calculated using DFT, plotting the band structure along the high-symmetry points and the density of states (DOS) to investigate the electronic response. To study magnetic behavior, the spin-up and spin-down electron distributions near the Fermi level are examined using the DOS versus energy plot. The partial density of states (PDOS) is analyzed to identify which orbitals contribute most or least to the electronic states. Based on the DFT-derived electronic structure, the frequency-dependent dielectric function ε(ω) is computed using the random phase approximation (RPA) [29, 30]. The real part, $\varepsilon_1(\omega)$, is obtained via the Kramers-Kronig relation [31], while the imaginary part, $\varepsilon_2(\omega)$, is derived from direct inter-band transitions. These dielectric functions are further used to calculate optical conductivity, reflectivity, energy-loss function, extinction coefficient, absorption coefficient, and refractive index. Optical anisotropy is assessed by analyzing these properties along different principal components of the dielectric tensor (E_{xx}, E_{yy}, E_{zz}).

3. RESULTS AND DISCUSSION

In this section, we discuss the key findings of the present study.

3.1 Structural Properties

The unit cell of the Hf_2CdN MAX-phase compound belongs to the space group $P6_3/mmc$ is shown in Fig. 1.

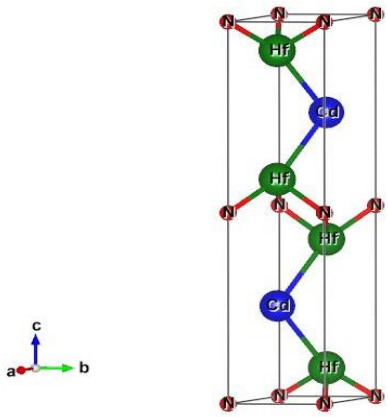

Fig. 1: (Colour online) the optimized and relaxed unit cell structure of Hf_2CdN MAX phase compound.

By analyzing the lattice parameters, bond lengths, and minimum ground-state energies, we studied the structural properties of Hf_2CdN. The calculations are performed using the GGA with PBE functional. The relaxed structure of Hf_2CdN is prepared for these calculations. The lattice parameters are initially calculated using the PBE functional and found to be a=b=3.295 Å and c=15.05 Å. The bond lengths between Hf–Cd, Cd–N, and Hf–N are also calculated using the PBE functional and found to be 3.155 Å, 4.217 Å, and 2.273 Å, respectively, before relaxation. After relaxation, the lattice parameters are determined to be a=b=3.2598 Å and c=14.6725 Å, while the bond lengths between Hf–Cd, Cd–N, and Hf–N are 3.1058 Å, 4.122 Å, and 2.230 Å, respectively.

Table 1: The estimated values of lattice parameters and bond lengths of nearest two atoms present in the material for PBE functional of optimized and relaxed structures of Hf_2CdN.

Estimated parameters	Present work Hf_2CdN	Reported work [33]
Lattice Parameter a = b (Å)	3.2598	3.1760
Lattice Parameter c (Å)	14.6725	14.4530
Bond Length Hf-Cd(Å)	3.1058	
ond Length Cd-N(Å)	4.1220	
Bond Length Hf-N(Å)	2.2300	
Bond Length Hf-C(Å)		
Bond Length Cd-C(Å)		

These values are in good agreement with previously reported values for211-based MAX-phase compounds [32]. In addition, the ground-state energy of Hf_2CdN is calculated using the PBE functional and found to be –64.716 eV, which is in good agreement with previously reported values [32]. This relatively low energy indicates a high binding energy, as binding energy and ground-state energy are inversely related. This reflects a tightly bound structure, confirming that the material is structurally stable. Based on the calculated bond lengths, lattice parameters, and ground-state energy, the stability of the material is further confirmed. All the estimated structural data are presented in Table 1.

3.2 Mechanical Properties

The mechanical properties are investigated based on the values of elastic parameters and the modulus of rigidity. The mechanical stability and strength of the MAX phase compound under compression are analyzed after applying a certain amount of pressure to the material. In the present work, we have explored the mechanical properties of the Hf_2CdN MAX phase compound using different elastic constants. The mechanical stability of the MAX phase compound can be confirmed by the Born stability criterion. Since the Hf_2CdN compound has a hexagonal structure, it consists of five independent elastic constants: C_{11}, C_{12}, C_{13}, C_{33}, and C_{44}. The compound is considered mechanically stable if it satisfies the Born stability criteria given by equations (1), (2), (3) & (4), [34]:

$C_{11} > |C_{12}|$ . . . (1)

$2C^2_{13} < C_{33}(C_{11} + C_{12})$ . . . (2)

$C_{44} > 0$ . . . (3)

$C_{66} > 0 >$ . . . (4)

The elastic constants of the Hf_2CdN compound satisfy the Born stability criteria and, hence, the material is mechanically stable. For evaluating different mechanical properties, we used the Voigt-Reuss-Hill approximations [24, 25, 26]. The bulk modulus (B), shear modulus (G), and Young's modulus (E) collectively referred to as moduli of rigidity are calculated using equations (5), (6), and (7), respectively [35]:

$B = \frac{2}{9}(c_{11} + c_{12} + \frac{2C_{12}+C_{33}}{2})$ . . . (5)

$G = \frac{1}{30}(7C_{11} + 2C_{12} - 4C_{13} - 5C_{12} + 12C_{44})$ . . . (6)

$E = \frac{9BG}{3B+G}$ . . . (7)

Using the PBE functional, the values of B, G, and E for the Hf_2CdN compound are found to be 143.72 GPa, 90.44 GPa, and 224.28 GPa, respectively. The high values of the module of rigidity indicate that a large amount of force is required to deform the material. Thus, the Hf_2CdN compound exhibits high rigidity, meaning it resists deformation and tends to retain its original shape. The positive or negative value of the Cauchy pressure denotes the bonding nature of any MAX phase compound [36]. For Hf_2CdN, the Cauchy pressure is found to be -2.8 GPa (negative), indicating metallic-like bonding. The anisotropic nature of the compound is determined by the universal anisotropic index, given by equation (8), [27]:

$A_u = 5(\frac{G_V}{G_R}) + (\frac{B_V}{B_R}) - 6$ . . . (8)

Here, G_V and $G_R$represent the shear modulus, while B_V and $B_R$represent the bulk modulus for the Voigt and Reuss approximations, respectively. If the value of the universal anisotropic index is positive, the compound is considered anisotropic [27]. We found the value of the universal anisotropic index to be 0.12, indicating the anisotropic nature of Hf_2CdN. The Vickers hardness coefficient, which measures the hardness of a compound, is given by equation (9) [37]:

$$H_v = 0.92\left(\frac{G}{B}\right)^{1.137} G^{0.708} \quad \ldots . (9)$$

Typically, MAX phase compounds have a Vickers hardness greater than 2 GPa [37]. Supporting this fact, the Vickers hardness (H_v) is found to be 13.188 GPa, 12.818 GPa, and 13.866 GPa using the Voigt, Reuss, and Hill approximations, respectively. These values further confirm the hardness of the Hf_2CdN compound. Based on the Kleinman parameter (ζ), the resistance to deformation (either bending or stretching) can be determined. If the value of ζ is greater than 0.5, the material exhibits stretching behavior, whereas a value less than 0.5 indicates bending behavior [37]. The parameter is given by equation (10) [37, 38]:

$\zeta = \frac{2C_{11}+8C_{12}}{7C_{11}+2C_{12}}$ . . . (10)

The ζ value of 0.48 for Hf_2CdN, being less than 0.5, indicates a bending-resistant nature for the PBE functional. Using Pugh's ratio and Poisson's ratio, we can determine whether the compound is brittle or ductile [39]. Pugh's and Poisson's ratios are given by equations (11) and (12), respectively [39]:

Pugh's ratio = $\frac{B}{G}$ . . . . (11)

Poisson's ratio (б) = $\frac{3B-2G}{2(3B+G)}$ . . . . (12)

Poisson's ratio greater than 0.26 indicates the ductile nature of a MAX phase compound, while a value less than 0.26 signifies brittleness [39]. Based on our analysis, the Poisson's ratios are found to be 0.240, 0.241, and 0.241 for the Voigt, Reuss, and Hill approximations, respectively, confirming the brittle nature of the Hf_2CdN compound. Similarly, for Pugh's ratio, a value less than 1.75 indicates brittleness, whereas a value greater than 1.75 represents ductility [39]. We obtained Pugh's ratio values of 1.59, 1.61, and 1.59 for the Voigt, Reuss, and Hill approximations, respectively. These values indicate that the compound under investigation exhibits a brittle nature. The Table 2 and Table 3 presents the stiffness tensor and estimated value of modulus of rigidities, Poisson ratio, Pugh's ratio, and Vickers Hardness coefficient with Voigt, Reuss, and Hill approximations of the Hf_2CdN MAX phase compound.

Table 2: the estimated values of stiffness tensors (C_{ij}) GPa of Hf_2CdN MAX phase compound for PBE functional.

C_{ij} (i/j)	1	2	3	4	5	6
1	289.16	76.77	83.71	0.00	0.00	0.00
2	76.77	289.19	83.71	0.00	0.00	0.00
3	83.71	83.71	226.72	0.00	0.00	0.00
4	0.00	0.00	0.00	79.52	0.00	0.00
5	0.00	0.00	0.00	0.00	79.52	0.00
6	0.00	0.00	0.00	0.00	0.00	106.21

Table 3: the calculated values of bulk modulus (B), Young modulus (E), shear modulus (G) Poisson ratio (б), Pugh's ratio (B/G), and Vickers Hardness coefficient (H_v) of Hf_2CdN compound with Voigt, Reuss, and Hill approximations.

Mechanical Properties	Voigt	Reuss	Hill
B (Gpa)	143.72	142.31	143.01
E (Gpa)	224.28	219.95	222.12
G (Gpa)	90.44	88.52	89.41
б	0.24	0.24	0.24
B/G	1.59	1.61	1.59
H_v(Gpa)	13.11	12.69	12.90

3.3 Optical Properties

When electromagnetic radiation interacts with the surface of a material, phenomena such as reflection, refraction, and polarization occur [40]. A detailed and precise study of optical properties opens the door to numerous potential applications in various sectors, including energy storage, optoelectronics, and

sensing devices [2, 23]. In this work, based on the electronic structure derived from DFT, the random phase approximation (RPA) is used to compute the frequency-dependent dielectric function, ε(ω) [41]. In this section, we discuss the optical properties of the Hf_2CdN MAX phase compound by analyzing its dielectric functions (tensors), reflection coefficient, refraction coefficient, energy loss function, and extinction coefficient. We analyzed the real and imaginary parts of the dielectric function over a photon energy range of 0 to 25 eV. For other optical properties, different ranges of photon energies are used. In each plane, the dielectric tensor is an important concept that measures the dielectric response when an electric field is applied. Mathematically, the complex dielectric function is expressed as;

$$\varepsilon(\omega) = \varepsilon_1(\omega) + i\varepsilon_2(\omega) \ldots \quad (13)$$

where $\varepsilon_1(\omega)$is the real part of the dielectric function (real component of the dielectric tensor) and $\varepsilon_2(\omega)$is the imaginary part (imaginary component of the dielectric tensor) [42]. The real part, $\varepsilon_1(\omega)$, is obtained using the Kramers–Kronig relation, while the imaginary part, $\varepsilon_2(\omega)$, was evaluated from direct inter-band transitions [31]. These components are used to calculate optical conductivity, reflectivity, energy-loss function, extinction coefficient, absorption coefficient, and refractive index, which are essential for investigating optical properties. We analyzed these optical properties for the different principal components of the dielectric tensor (E_{xx}, E_{yy}, E_{zz}) to confirm the optical anisotropy of the material. Mathematically the real dielectric function $\varepsilon_1(\omega)$ and imaginary dielectric function $\varepsilon_2(\omega)$ is given by equations (14) & (15) respectively, [43, 44]:

$$\varepsilon_1(\omega) = 1 + \frac{2}{\pi} p \int_0^{\infty} \frac{\omega' \varepsilon_2(\omega')}{\omega'^2 - \omega^2} d\omega' \quad \ldots (14), \text{ and}$$

$$\varepsilon_2(\omega) = \frac{8}{2\pi\omega^2} \int \sum_{fi} \{Pfi(K)\}^2 \frac{\mathrm{dsk}}{\nabla\omega fi(K)} \quad \ldots (15)$$

The real part of the dielectric tensor, or the real dielectric function, describes the energy-storing capacity or polarization of a material. Figure 2 shows the real dielectric function versus photon energy, with the dielectric function plotted on the y-axis and the corresponding photon energies on the x-axis. We analyzed the graph in two cases: first, the variation of dielectric properties when the applied field is perpendicular to the plane of the material (E_{xx}, E_{yy} in-plane) and second, when the applied field is parallel to the plane of the material (E_{zz} out-of-plane). When a material is subjected to an electric field, its ions become polarized and shift slightly. The greater the applied field, the greater the polarization, and consequently, the higher the energy-storing capacity. The plot shows a non-zero value of the real dielectric function at zero photon energy, indicating that the material can store energy even in the absence of light. This behavior is due to the presence of metallic bonding between Hf and N and the bond between Hf and Cd. Several peaks appear in the (0-3) eV photon energy range, and the peak values of the real dielectric function arise due to resonance effects. At low frequencies, the energy is small, which allows both lighter and bound electrons to contribute to polarization, resulting in maximum polarization. Conversely, at high frequencies, the heavier or tightly bound electrons cannot respond effectively to the applied field, leading to reduced polarization. Beyond a certain frequency, the material no longer interacts with light and becomes transparent. The negative values observed at the plasma frequency indicate the metallic nature of the compound. In these regions, the material does not store energy. We found that the real dielectric function reaches its maximum value of 39.80 at nearly 0 eV photon energy for $E_{xx} = E_{yy}$. The graph then sharply decreases, showing some peaks in the infrared region, and becomes negative in the visible region. For E_{zz}, the graph starts from zero, reaches a maximum value of 33.21 at approximately 1.30 eV photon energy, and then sharply decreases, becoming negative at 1.75 eV. As the photon energy increases further, the graph exhibits several peaks in the visible and ultraviolet regions. Beyond this range, the dielectric function gradually disappears. From the analysis, we found that the maximum dielectric function occurs for $E_{xx} = E_{yy}$. Fig. 2 illustrated the variation of real dielectric function with the different values of photon energies of considered compound.

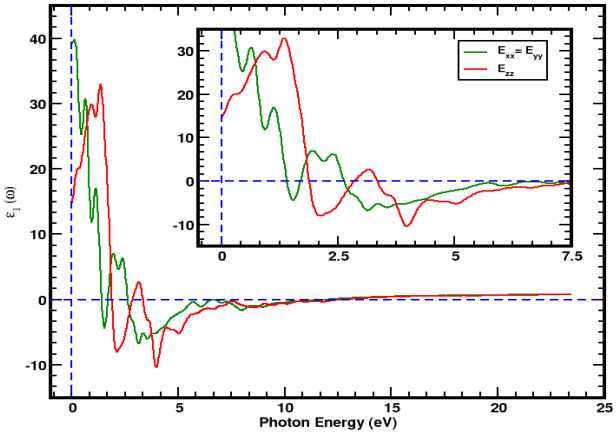

Fig. 2: (Colour online) the variation of real dielectric function with the photon energy of Hf_2CdN MAX phase compound for PBE functional. The inset represents the zoom scale of the real dielectric function versus photon energy plot.

The imaginary part of the dielectric function describes the absorption or energy loss that occurs when the electrons in a material are exposed to light (photons). This phenomenon arises due to inter-band transitions [45], which occur when the photon energy is exactly equal to the energy required for electrons to jump from the occupied valence band to the unoccupied conduction band. At this point, resonance occurs, resulting in peaks appearing in the (0-3) eV range, corresponding to the low-frequency region. The negative value near 0 eV photon energy indicates the metallic nature of the compound. Beyond a photon energy of approximately 10 eV, the material becomes transparent, meaning that light no longer affects the material and no energy loss occurs. A zero value of the imaginary dielectric function indicates that no inter-band transitions occur at that photon energy. For $E_{xx} = E_{yy}$, the graph exhibits several peaks in the infrared and visible regions, reaching a maximum of 28.54 at around 1.8 eV photon energy. For Ezz, the curve starts from a negative value, rises sharply to a maximum of 38.57 at approximately 2.3 eV, and then begins to decrease. Several peaks are also observed in the ultraviolet region; however, at higher photon energies, the curve vanishes. The maximum value of the imaginary dielectric function is found for E_{zz}. In both cases of the dielectric function, we found from the graphs that the dielectric function responds primarily at low photon energy. Fig. 3 Illustrated the variation of imaginary dielectric function with the different values of photon energies of considered compound.

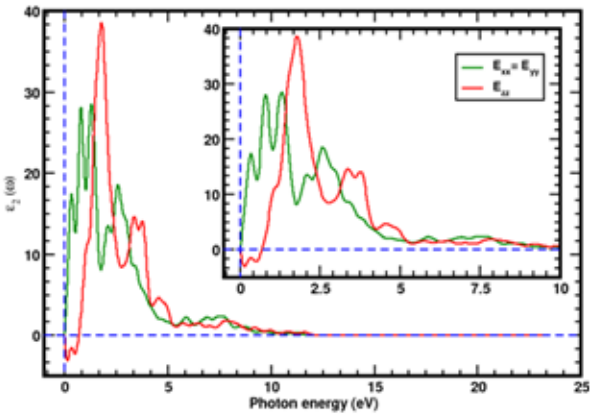

Fig. 3: (Colour online) the variation of imaginary dielectric function with the photon energy of Hf_2CdN MAX phase compound for PBE functional. The inset represents the zoom scale of the imaginary dielectric function versus photon energy plot.

The absorption coefficient determines how strongly a material absorbs light at a given photon energy [46]. A high absorption coefficient means that photons are quickly absorbed by the material, whereas a low absorption coefficient indicates that photons of that frequency can penetrate deeper into the material. Several peaks also appear in the spectrum due to inter-band transitions. The plot of the absorption coefficient, α(ω), versus photon energy is shown in Fig. 4.

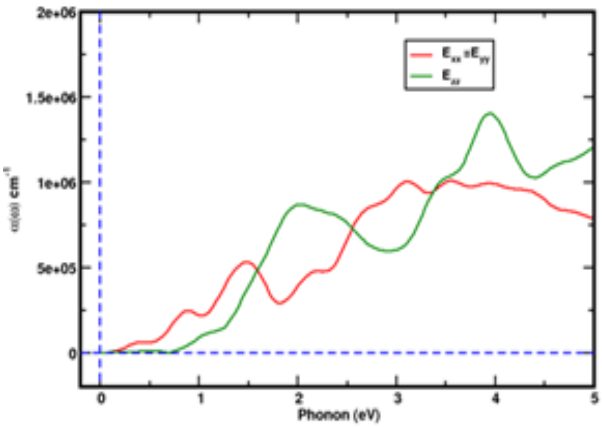

Fig. 4: (Colour online) the variation of absorption coefficient with the photon energy of Hf_2CdN MAX phase compound for PBE functional**.**

The absorption coefficient, α(ω), is plotted along the y-axis against photon energy on the x-axis. We calculated α(ω) using the following equation (16), [40]:

$$(\omega) = \frac{2\omega}{C}\left(\frac{\sqrt{\varepsilon_1^2+\varepsilon_2^2}}{2} - \frac{\varepsilon_1}{2}\right) \quad \ldots (16)$$

Analyzing the graph, the absorption coefficient of Hf_2CdN reaches a maximum in the ultraviolet region, with a value of 1.0024×10^6 for $E_{xx} = E_{yy}$. For E_{zz}, the maximum value is 1.4305×10^6, observed in both the ultraviolet and visible regions. The highest peak occurs for E_{zz} in the ultraviolet region.

Reflectivity determines how much light is reflected from the surface of a material when electromagnetic waves interact with it [32]. It also provides information about the electronic and optical response of the material [40]. A non-zero reflectivity indicates the presence of free electrons, suggesting metallic character. The reflectivity at 0 eV photon energy is called the static reflectivity, which Hf_2CdN exhibits. Several peaks appear in the spectrum due inter-band transitions. The plot of reflectivity, R(ω), versus photon energy is shown in Fig. 5.

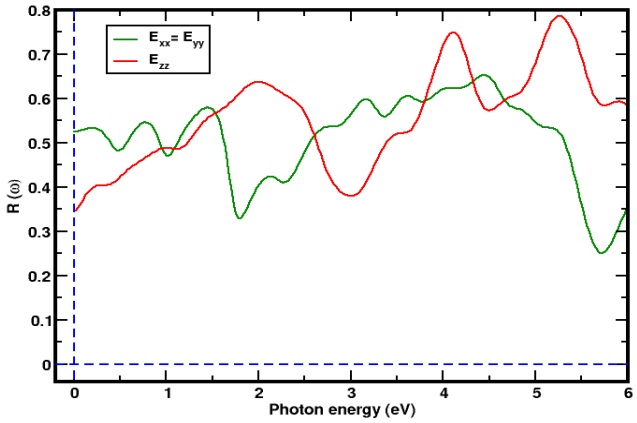

Fig. 5: (Colour online) the variation of reflection coefficient with the photon energy of Hf_2CdN MAX phase compound for PBE functional.

The reflectivity is plotted along the y-axis, and the corresponding photon energy is plotted along the x-axis. The reflection coefficient, R(ω), is calculated by equation (17), [47]:

$$R(\omega) = \frac{(\eta-1)^2+K^2}{(\eta+1)^2+K^2} \quad \ldots (17)$$

It is observed that the maximum reflectivity of Hf_2CdN for $E_{xx} = E_{yy}$ occurs in the ultraviolet region, with a value of 0.65, meaning that 35% of the light is absorbed by the material. For E_{zz}, the maximum reflectivity occurs at 5.5 eV photon energy, beyond the ultraviolet region, with a value of 0.78, indicating that 22% of the light is absorbed. For both $E_{xx} = E_{yy}$ and E_{zz}, several peaks are observed in the infrared, visible, and ultraviolet regions. The maximum reflectivity is found for E_{zz}.

The energy-loss function measures the inelastic scattering of electrons, since the imaginary part of the dielectric function describes how a material absorbs energy [40]. The important optical property, the energy-loss function characterizes the energy lost by an electron as it moves rapidly through a material, indicating how electrons (or photons) dissipate energy within the material. Due to the static response, the energy loss is very low at low frequencies or low photon energy. Figure 6 shows the plot of the energy-loss function, L(ω), versus photon energy, with L(ω) plotted along the y-axis and photon energy along the x-axis. The energy-loss function is mathematically expressed by equation (18), [38, 40]:

$$L(\omega) = \frac{\varepsilon_2}{\varepsilon_1^2+\varepsilon_2^2} \quad \ldots (18)$$

In the photon energy range of approximately (6-7) eV, we found the maximum energy-loss value for $E_{xx} = E_{yy}$, which is 0.68. Similarly, for E_{zz}, the maximum energy loss value is 0.50, observed in the (7-8) eV range. For all response axes, the maximum energy loss occurs in the (5-7) eV region. Overall, the highest energy-loss value is found for $E_{xx} = E_{yy}$.

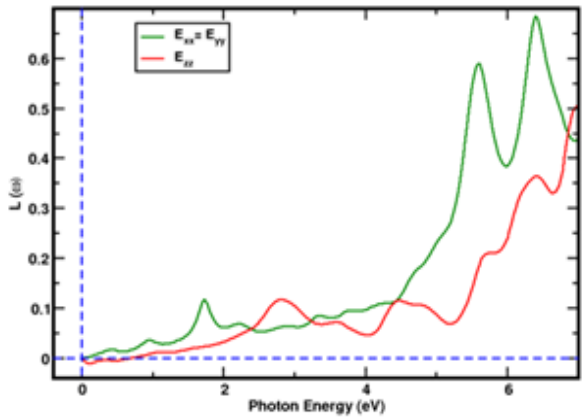

Fig. 6: (Colour online) the variation of energy loss function with the photon energy of Hf_2CdN MAX phase compound for PBE functional.

The refractive index describes how light propagates through a material [44]. It is directly related to the real part of the dielectric function, and the extinction coefficient [48]. Due to the metallic nature of the material, the refractive index is non-zero at 0 eV photon energy, which is referred to as the static refractive index. A high refractive index indicates that light travels more slowly inside the material than in a vacuum. By analyzing the refractive index of a material, we can predict the bending behavior of light and electromagnetic radiation as it passes through the material. The refractive index of considered material is calculated by using equation (19), [40]:

$$\eta(\omega) = \left(\frac{\sqrt{\varepsilon_1^2+\varepsilon_2^2}}{2} + \frac{\varepsilon_1}{2}\right)^{\frac{1}{2}} \quad \ldots (19)$$

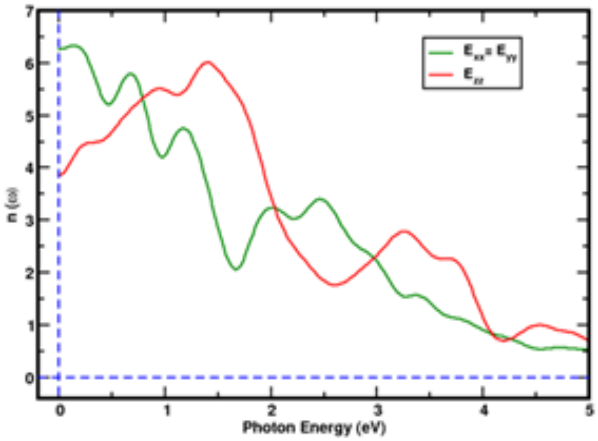

Fig. 7: (Colour online) the variation of refractive index with the photon energy of Hf_2CdN MAX phase compound for PBE functional.

Fig. 7 shows the plot of the refractive index η(ω), versus the corresponding photon energy. The maximum refractive index is observed in the infrared region, with a value of approximately 6.34 for $E_{xx} = E_{yy}$. For E_{zz}, the maximum value is about 6.04, also in the infrared region. Several peaks appear as the photon energy increases. Overall, the refractive index is highest for $E_{xx} = E_{yy}$.

The extinction coefficient describes the level of absorption loss experienced by electromagnetic waves as they travel through a material. Fig. 8 shows the plot of the extinction coefficient versus photon energy, with the extinction coefficient plotted along the y-axis and the corresponding photon energy along the x-axis. The extinction coefficient is calculated using the equation (20), [40]:

$$K(\omega) = \left(\frac{\sqrt{\varepsilon_1^2+\varepsilon_2^2}}{2} - \frac{\varepsilon_1}{2}\right)^{\frac{1}{2}} \quad \ldots (20)$$

For $E_{xx} = E_{yy}$, the maximum value of the extinction coefficient is observed to be approximately 3.95 in the (1-2) eV region, whereas for E_{zz}, the maximum value is around 4.34 in the visible region. At nearly 0 eV photon energy, a non-zero extinction coefficient is observed, reflecting the metallic nature of the compound. The higher value of E_{zz} compared to $E_{xx} = E_{yy}$ indicates the layered nature of the crystal, where electronic states along the c-axis couple differently. From all the plots and values presented, we conclude that the Hf_2CdN compound exhibits anisotropic properties, as $E_{xx} = E_{yy}$ but is not equal to E_{zz}, based on the PBE functional.

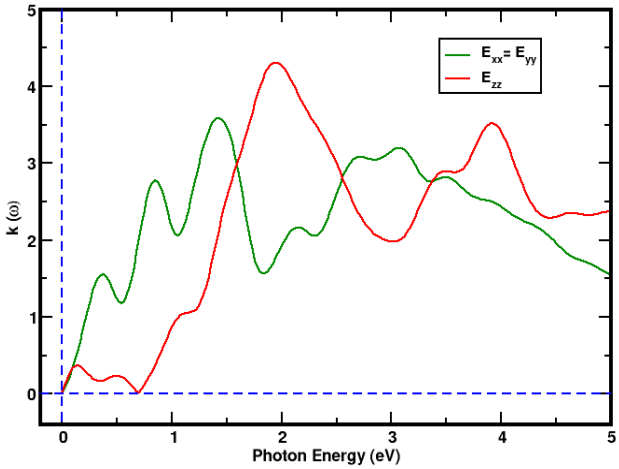

Fig. 8: (Colour online) the variation of extinction coefficient with the photon energy of Hf_2CdN MAX phase compound for PBE functional.

3.4 Magnetic Properties

Magnetic materials have a wide range of applications in both academic and industrial fields [49, 50]. In this work, we examined the magnetic properties of the Hf_2CdN MAX phase compound using density of states (DOS) and partial density of states (PDOS) plots, employing the PBE functional in DFT calculations. Each atomic orbital in the material contains electrons with up- and down-spin states. The distribution of these spin states determines the magnetic moment of the material. At the Fermi energy level, if the up- and down-spin states are distributed symmetrically, the material will have a zero magnetic moment, indicating that the material is non-magnetic [51, 52]. Similarly, if the up- and down-spin states of electrons are not distributed symmetrically around the Fermi energy level, the material will have a nonzero magnetic moment, indicating that it is magnetic. The DOS plot of Hf_2CdN, with energy (eV) on the x-axis and density of states (DOS) on the y-axis, is shown in Fig. 9.

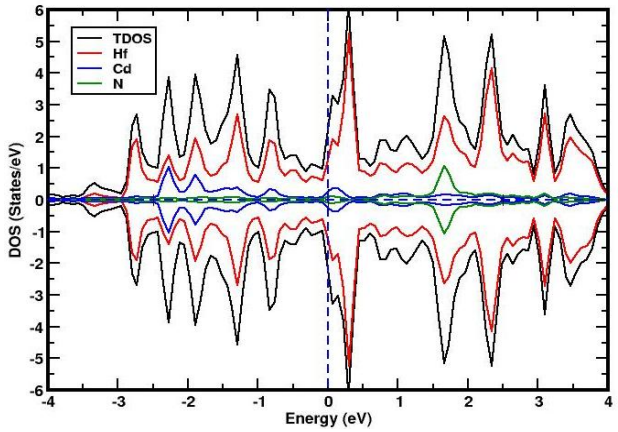

Fig. 9: (Color online) density of states (DOS) of Hf_2CdN MAX phase compound, where vertical blue dotted line represents Fermi energy level and horizontal blue dotted line separates up- and down-spin states.

The vertical blue dotted line represents the Fermi energy level, and the horizontal blue dotted line separates the up- and down-spin states. From the DOS plot computed using the PBE functional, around the Fermi energy level, the up- and down-spin states of electrons are distributed symmetrically. Therefore, we conclude that the material is non-magnetic. The total density of states (TDOS), represented by the black curve in the plot, also shows a symmetrical distribution of up- and down-spin states, confirming the non-magnetic nature of the Hf_2CdN compound.

Furthermore, the magnetic properties of a material arise from the different spin states (up and down) of its electrons. The partial density of states (PDOS) provides insight into the contributions of specific electron orbitals to the magnetic moment. Fig. 10 shows the PDOS plot of Hf_2CdN calculated using the PBE functional. From the plot, it is evident that the 6s, $5p_x$, $5p_y$, $5p_z$, $5d_{xy}$, $5d_{x^2-y^2}$, $5d_{xz}$, $5d_{yz}$ orbitals of the Hf atom have spin states distributed symmetrically around the Fermi level.

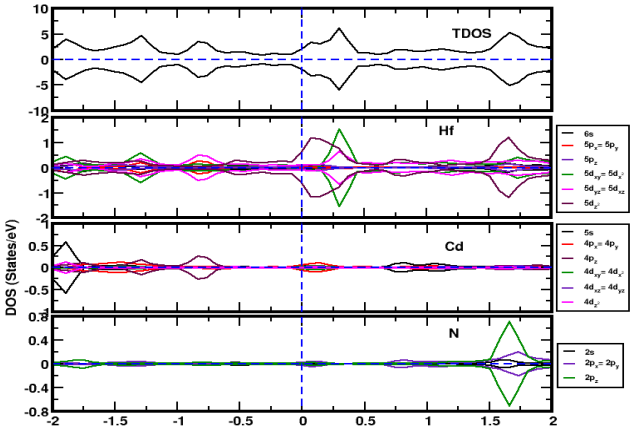

Fig. 10: (Color online) partial density of states (PDOS) of Hf_2CdN MAX phase compound, where vertical blue dotted line represents Fermi energy level and horizontal blue dotted line separates up- and down-spin states.

Although the $5d_z^2$ orbital of Hf also has a symmetrical distribution around the Fermi level, it contributes the highest magnetic moment, with values of $0.31\mu_B$/cell and $-0.31\mu_B$/cell for the up- and down-spin states, respectively. Similarly, the 5s, $4p_x$, $4p_y$, $4p_z$, $4d_{xy}$, $4d_{x^2-y^2}$, $4d_{xz}$, $4d_{yz}$, $4d_z^2$ orbitals of Cd and the 2s, $2p_x$, $2p_y$, $2p_z$ orbitals of N show symmetrical contributions around the Fermi level. Notably, the orbitals of the N atom contribute almost nothing to the magnetic moment, with the $2p_z$ orbital giving the maximum contribution of 0.05 μ_B/cell. For the Cd atom, the $4p_z$ orbital has the maximum contribution of 0.04 μ_B/cell for both spin-up and spin-down electrons. As a result, the Hf_2CdN compound exhibits non-magnetic properties.

The Table 4 shows the magnetic moments contributed by the individual orbital of Hf, Cd, and N atoms in the Hf_2CdN MAX phase compound.

Table 4: The calculated values magnetic moment (μ) contributed by each orbital of Hf, Cd and N atom in Hf_2CdN compound.

Orbitals	μ of up-spin (μ_B/cell)	μ of down-spin (μ_B/cell)	μ of Resultant (μ_B /cell)
2s of N	0.0087	-0.0087	0.0000
$2p_x$ of N	0.0321	-0.0321	0.0000
$2p_y$ of N	0.0321	-0.0321	0.0000
$2p_z$ of N	0.0518	-0.0518	0.0000
5s of Cd	0.0474	-0.0474	0.0000
$4p_x$ of Cd	0.0319	-0.0319	0.0000
$4p_y$ of Cd	0.0319	-0.0319	0.0000
$4p_z$ of Cd	0.0400	-0.0400	0.0000
$4d_{xy}$ of Cd	0.0083	-0.0083	0.0000
$4d_x^2$ of Cd	0.0083	-0.0083	0.0000
$4d_{yz}$ of Cd	0.0072	-0.0072	0.0000
$4d_{xz}$ of Cd	0.0072	-0.0072	0.0000
$4d_x^2$ of Cd	0.0110	-0.0110	0.0000
6s of Hf	0.0524	-0.0524	0.0000
$5p_x$ of Hf	0.0448	-0.0448	0.0000
$5p_y$ of Hf	0.0448	-0.0448	0.0000
$5p_z$ of Hf	0.0428	-0.0428	0.0000
$5d_x^2$ of Hf	0.2260	-0.2260	0.0000
$5d_{xy}$ of Hf	0.2260	-0.2260	0.0000
$5d_{xz}$ of Hf	0.2033	-0.2033	0.0000
$5d_{yz}$ of Hf	0.2033	-0.2033	0.0000
$5d_z^2$ of Hf	0.3100	-0.3100	0.0000

3.5. Electronic Properties

To predict the electronic properties of a material, it is essential to analyze its band structure and density of states (DOS) plots. In the present work, we computed and analyzed the band structure and DOS of Hf_2CdN using the DFT method with the PBE functional. Fig. 11 shows the band and DOS plots of the compound under consideration.

High-symmetry points are plotted along the x-axis, while the corresponding energies are plotted along the y-axis. The vertical green dotted lines parallel to the y-axis represent the high-symmetry points (Γ, H, K, Γ, A, L, H). The horizontal green line parallel to the x-axis represents the Fermi level, which separates

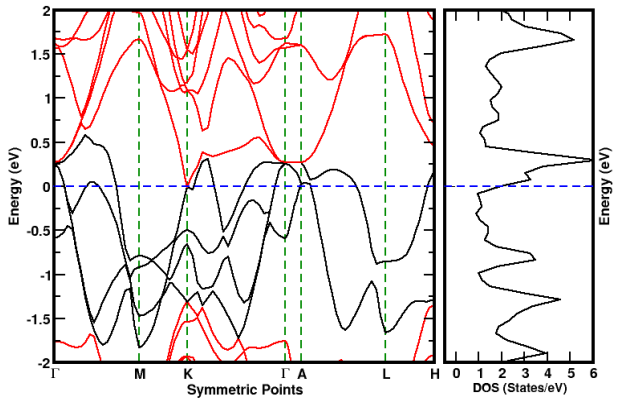

Fig. 11: (Color online) band structure and density of states (DOS) plots of Hf_2CdN MAX phase compound, where horizontal dotted line separates the electronic band in band structure and vertical dotted lines represent the highly symmetrical points.

the valence and conduction bands. The valence band is located below the Fermi level, and the conduction band is located above it. Analyzing the band and DOS plots, it is observed that some of the bands, shown in black, cross the Fermi energy level. This indicates that the valence band maximum and the conduction band minimum are identical, implying a zero-band gap, which reflects the metallic nature of the material. In the band structure, several bands cross the Fermi energy level, indicating the presence of charge carriers (electrons or ions) that can move freely across the Fermi level. Additionally, the DOS plot shows unoccupied energy states appeared near the Fermi level, suggesting a probability of charge carriers occupying these states. These observations further confirm that the Hf_2CdN compound is metallic. Based on the results from both the DOS and band structure plots, we concluded that Hf_2CdN exhibits metallic behavior.

The band structure and DOS analyses confirm the metallic character of the compound, which arises from the presence of free electrons at the Fermi level. These charge carriers play a key role in determining the material's optical behavior. In metals, the lack of a band gap results in strong intrabank transitions, causing high reflectivity and low transmittance in the low-energy region. Additionally, the negative real part of the dielectric function at lower photon energies further supports the metallic nature. Thus, the optical response of the material is in good agreement with its electronic structure, where the high density of electronic states near the Fermi level governs the observed absorption and reflectivity features.

3.6. Dynamical Properties

The dynamical stability of the Hf_2CdN MAX phase compound is examined using its phonon dispersion curve. Fig. 12 shows the phonon frequency curve of the Hf_2CdN compound.

The highly symmetric points (Γ, H, K, Γ, A, L, H) are plotted along the x-axis, with phonon frequencies plotted along the y-axis. In the curve, each vertical dotted line corresponds to a high-symmetry point. The dynamical stability of the compound is evaluated using the phonon frequency curve at each symmetric point [46]. We observed that all frequencies are positive, indicating dynamical stability. Each unit of the MAX phase contains eight atoms, resulting in a total of twenty-four phonon branches, of which there are acoustic and twenty-one are optical. The optical branches, located at the higher frequency range, determine the optical behavior of the compound, while the acoustic branches, located at the lower frequency range, correspond to coherent vibrations of atoms. Optical vibrations arise from out-of-phase atomic motions, whereas acoustic vibrations result from in-phase atomic motions [46]. For Hf_2CdN, the optical branches appear above 2 cm^{-1}. From the phonon frequency curve, all frequencies at every symmetric point are positive, confirming the dynamical stability of the compound. In Figure 12, the green curve represents the acoustic bands, and the red curve represents the optical bands. This confirms that the Hf_2CdN compound is dynamically stable. Additionally, we observe that the frequency of the acoustic modes for Hf_2CdN is zero at the Γ point, which further confirms the dynamical stability of the compound.

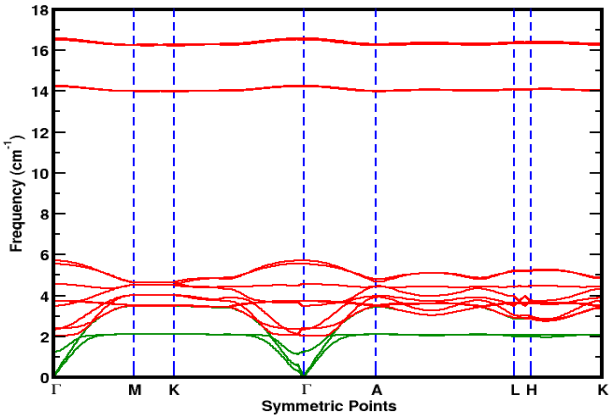

Fig. 12: (Color online) phonon frequency curve of Hf_2CdN MAX phase compound, highly symmetric points (Γ, H, K, Γ, A, L, H) are plotted along the x axis and corresponding photon frequency are plotted along the y-axis.

4. CONCLUSIONS

We have investigated the structural, mechanical, optical, magnetic, electronic, and dynamical properties of Hf_2CdN compound by employing density functional theory (DFT) with the GGA–PBE functional. For the structural properties, we computed the bond lengths, lattice parameters, and ground-state energy. The computed values are in good agreement with those reported values for other stable 211 MAX phase compounds, confirming that Hf_2CdN is structurally stable. For mechanical stability, we calculated and analyzed various moduli and elastic constants. The Born stability criteria are satisfied by Hf_2CdN, indicating that the compound is mechanically stable. The Zener anisotropy index is found to be -3.03, which deviates from 1, suggesting anisotropic behavior. The Cauchy pressure is computed -2.80, implying metallic-like bonding. Pugh's ratio and Poisson's ratio are less than 1.75 and 0.26, respectively, confirming the brittle nature of the compound. Based on the Vickers hardness and Kleinman parameter, we conclude that Hf_2CdN exhibits significant hardness and bond-stretching characteristics. For optical properties, we plotted the variation of photon energy with the real dielectric function, extinction coefficient, reflection, absorption coefficient, refractive index, and energy loss function. The maximum energy loss occurs in the UV region and beyond, compared to the infrared and visible regions. The refractive index and extinction coefficient

are higher in the infrared region, suggesting high optical conductivity. The reflectivity analysis shows that Hf_2CdN has a high reflection coefficient at low photon energies and in the UV region, indicating its potential use as a radiation-shielding material. A high absorption coefficient is observed in the visible and UV regions, suggesting possible applications in optoelectronic devices. The strong reflectivity in the UV region further highlights its suitability for UV mirrors and radiation-shielding materials. The high refractive index in the infrared region also supports its potential for optoelectronic applications. Overall, the compound shows strong optical response even at low photon energy. Since the phonon frequency curve exhibits only positive frequencies at all high-symmetry points, Hf_2CdN is dynamically stable. The electronic properties are investigated using band structure and DOS plots. The band structure reveals several bands crossing the Fermi energy level, indicating a very small or nearly zero bandgap energy. The DOS at the Fermi level is nonzero, confirming good electrical conductivity. From the DOS and PDOS analyses, we conclude that the compound is nonmagnetic due to the symmetrical distribution of spin-up and spin-down electron states around the Fermi energy level.

ACKNOWLEDGEMENTS

Authors would like to thank the condensed matter research lab CDP TU Kirtipur for conducting the computational work.

AUTHOR CONTRIBUTIONS

S. Timsina: Gathering information, data analysis and interpreting, making figures, writing the original manuscript. B. Dhital: Contribution to Formal analysis. Sushil Shrestha: Contribution to Formal analysis and editing the manuscript. D. Dhital: Contribution to Formal analysis. G. Paudel: Contribution to Formal analysis and editing the manuscript. O.S. Rijal: Contribution to Formal analysis and editing the manuscript. H.K. Neupane: Developed the concept, Supervised the investigation, analyzed the results, and implemented extensive revisions to the manuscript.

DATA AVAILABILITY

The data used to generate the figures and tables are available from the corresponding author upon request.

DECLARATIONS AND CONFLICT OF INTEREST

The author declares no known conflicts of interest.

REFERENCES

[1] M.S. Alam, M.A. Chowdhury, T. Khandaker, M.S. Hossain, M.S. Islam, M.M. Islam, M.K. Hasan, Advancements in MAX phase materials: structure, properties, and novel applications, *RSC Advances,* **14**(37) *(2024)* 1426995–7041. DOI: 10.1039/D4RA03714F

[2] H.K. Neupane, O.S. Rijal, R.K. Neupane, G. Paudel, P. Shrestha, S. Sharma, L.P. Joshi, R. Parajuli, Structural, dynamical, thermomechanical, electronic, magnetic, and optical properties of M_2 AC (M = Ta, Sc; A = Al, Cd) MAX phase compound Via DFT approach, *Physica Scripta,* **100** (2025) 095921. DOI 10.1088/1402-4896/adffc6

[3] [3] M.S. Alam, M.A. Chowdhury, M.A. Kowser, M.S. Hossain, M.S. Islam, M.M. Islam, M.K. Hasan, T. Khandaker, Advances of MAX phases: Synthesis, characterizations and challenges, *Engineering Reports,* **6** (2024) e12911. DOI: https://doi.org/10.1002/eng2.12911

[4] M.W. Barsoum, The $M_{N+1}AX_N$ phases: A new class of solids *Progress in Solid State Chemistry,* **28** (2000) 201–81. DOI: https://doi.org/10.1016/S0079-6786(00)00006-6

[5] P. Eklund, M. Beckers, U. Jansson, H. Högberg, L. Hultman, The $M_{N+1}AX$ phases: Materials science and thin-film processing *Thin Solid Films,* **518** (2010) 1851–78. DOI:https://doi.org/10.1016/j.tsf.2009.07.184

[6] M.A. Hadi, M.S. Ali, S. H. Naqib, A.K.M.A. Islam, Band structure, hardness, thermodynamic and optical properties of superconducting Nb_2AsC, Nb_2InC and Mo_2GaC, *International Journal of Computational Materials Science and Engineering,* **02** (2013) 1350007. DOI: https://doi.org/10.1142/S2047684113500073

[7] M. S. Ali, M. A. Rayhan, M. A. Ali, R. Parvin, and A. K. M. A. Islam, New MAX Phase Compound Mo_2TiAlC_2: First-principles Study, *arXiv Preprint arXiv:* **1603** (2016) 04215. DOI: https://doi.org/10.48550/arXiv.1603.04215.

[8] M. Roknuzzaman, M.A. Hadi, M.A. Ali, M.M. Hossain, N. Jahan, M.M. Uddin, J.A. Alarco, K. Ostrikov, First hafnium-based MAX phase in the 312 family, Hf_3AlC_2: A first-principles study *Journal of Alloys and Compounds,* **727** (2017) 616–26. DOI: https://doi.org/10.1016/j.jallcom.2017.08.151

[9] F. Sultana, M.M. Uddin, M.A. Ali, M.M. Hossain, S.H. Naqib, and A.K.M.A. Islam, First principles study of M_2InC (M = Zr, Hf and Ta) MAX phases: The effect of M atomic species, *Results in Physics*, **11** (2018) 869–876. DOI: https://doi.org/10.1016/j.rinp.2018.10.044

[10] M.A. Hadi, N. Kelaidis, S.H. Naqib, A. Chroneos, A.K.M.A. Islam, Mechanical behaviors, lattice thermal conductivity and vibrational properties of a new MAX phase Lu_2SnC, *Journal of Physics and Chemistry of Solids*, **129** (2019)162–171. DOI: https://doi.org/10.1016/j.jpcs.2019.01.009

[11] N. Miao, J. Wang, Y. Gong, J. Wu, H. Niu, S. Wang, K. Li, A. R. Oganov, T. Tada, H. Hosono, Computational Prediction of Boron-Based MAX Phases and MXene Derivatives, Chemistry of Materials, **32** (2020) 6947–6957. DOI: https://doi.org/10.1021/acs.chemmater.0c02139

[12] A. Yang, Y. Duan, L. Bao, M. Peng, L. Shen, Elastic properties, tensile strength, damage tolerance, electronic and thermal properties of TM_3AlC_2 (TM = Ti, Zr and Hf) MAX phases: A first-principles study, *Vacuum,* **206** (2022) 111497. https://doi.org/10.1016/j.vacuum.2022.111497

[13] A.A. Belkacem, H. Rached, M. Caid, Y. Rached, D. Rached, N. T. Mahmoud, N. Benkhettou, The stability analysis and efficiency of the new MAX-phase compounds M_3GaC_2 (M: Ti or Zr): A first-principles assessment, *Results in Physics,* **38** (2022) 105621. DOI: https://doi.org/10.1016/j.rinp.2022.105621

[14] M. Rougab, A. Gueddouh, First-principles insights into structural stability, elastic anisotropies, mechanical and thermodynamic properties of the Hf_2GeX (X = C, N, and B) 211 MAX phases, *Journal of Physics and Chemistry of Solids,* **176** (2023) 111251. https://doi.org/10.1016/j.jpcs.2023.111251

[15] B. Ul Haq, S.-H. Kim, A. Alqahtani, R. Ahmed, A.R. Chaudhry, Y.A.H. Obaidat, M.B. Kanoun, S. Goumri-Said, Investigations of the physical behavior of Cr_2PX (X = C and N) MAX phases through first-principles calculations, *Computational Condensed Matter,* **40** (2024) e00937. DOI: https://doi.org/10.1016/j.cocom.2024.e00937

[16] O.S. Rijal, H. K. Neupane, D. Oli, R.K. Neupane, P. Shrestha, S. Sharma, L.P. Joshi, R. Parajuli, A first-principles investigation of the structural, mechanical, dynamic, electronic, magnetic, and optical properties of Ti_2AC (A = Cd, S) MAX phase compounds, *J0urnal of Physics D: Applied Physics,* **58** *(2025)* 125102. DOI: 10.1088/1361-6463/ada808

[17] K.B. Lipkowitz, D.B. Boyd, *Reviews in Computational Chemistry*, **7** (1996). DOI:10.1002/9780470890905

[18] P. Giannozzi, O. Baseggio, P. Bonfà, D. Brunato, C. Car, I. Carnimeo, C. Cavazzoni, S. De Gironcoli, P. Delugas, F. Ferrari Ruffino, A. Ferretti, N. Marzari, I. Timrov, A. Urru, S. Baroni, QUANTUM ESPRESSO toward the exascale, *Journal of Chemical Physics,* **152** (2020) 154105. DOI: https://doi.org/10.1063/5.0005082

[19] B. Hammer, L.B. Hansen, J.K. Nørskov, Improved adsorption energetics within density-functional theory using revised Perdew–Burke–Ernzerhof functionals, *Physical Review B,* **59** (1999) 7413–7421. DOI: https://doi.org/10.1103/PhysRevB.59.7413

[20] A. Kokalj, XCrySDen-a new program for displaying crystalline structures and electron densities, *Journal of Molecular Graphics and Modeling,* **17** (1999) 176–179. DOI:https://doi.org/10.1016/S1093-3263(99)00028-5

[21] B.K.R. Sanapalli, V. Yele, S. Jupudi, V.V.S.R. Karri, Ligand-based pharmacophore modeling and molecular dynamic simulation approaches to identify putative MMP-9 inhibitors, *RSC Advances*, **11** (2021) 26820–26831. DOI: 10.1039/D1RA03891E

[22] H.J. Monkhorst, J. D. Pack, Special points for Brillouin-zone integrations, *Physical Review B,* **13** (1976) 5188–5192. DOI: https://doi.org/10.1103/PhysRevB.13.5188

[23] İ. Kars Durukan, Mechanical, vibration, and optical properties of IrAl intermetallic compound via DFT calculations: high-pressure effect, *Physica Scripta,* **98** (2023) 075903. DOI: 10.1088/1402-4896/acd904

[24] W. Voigt, Ueber die Beziehung zwischen den beiden Elasticitätsconstanten isotroper Körper, *Annals of Physics,* **274** (1889) 573–587. DOI: https://doi.org/10.1002/andp.18892741206

[25] A. Reuss, Berechnung der Fließgrenze von Mischkristallen auf Grund der Plastizitätsbedingung für Einkristalle, *Zeitschrift für Angewandte Mathematik und Mechanik,* **9** (1929) 49–58. DOI: https://doi.org/10.1002/zamm.19290090104

[26] R. Hill, The Elastic Behaviour of a Crystalline Aggregate, *Proceedings of the Physical Society A,* **65** (1952) 349–354. DOI 10.1088/0370-1298/65/5/307

[27] S.I. Ranganathan, M. Ostoja-Starzewski, Universal Elastic Anisotropy Index, *Physical Review Letters,* **101** (2008) 055504. DOI: https://doi.org/10.1103/PhysRevLett.101.055504

[28] L. Kleinman, Deformation Potentials in Silicon. I. Uniaxial Strain, *Physics Review,* **128** *(1962)* 2614–2621. DOI: https://doi.org/10.1103/PhysRev.128.2614

[29] W. Körner, C. Elsässer, First-principles density functional study of dopant elements at grain boundaries in ZnO, *Physics Review B,* **81** (2010*)* 085324. DOI: https://doi.org/10.1103/PhysRevB.81.085324

[30] G.P. Chen, V.K. Voora, M.M. Agee, S.G. Balasubramani, F. Furche, Random-Phase Approximation Methods, *Annual Review of Physical Chemistry,* **68** (2017) 421–445. DOI: https://doi.org/10.1146/annurev-physchem-040215-112308

[31] X. Li, H. Cui, R. Zhang, First-principles study of the electronic and optical properties of a new metallic MoAlB, *Scientific Reports,* **6** (2016) 39790. DOI: 10.1038/srep39790

[32] H.K. Neupane, D. Oli, O.S. Rijal, R.K. Neupane, P. Shrestha, S. Sharma, L.P. Joshi, R. Parajuli, Exploring the structural, dynamical, mechanical, electronic, magnetic, and optical properties of Ta_2AlN, Ti_2AlN & Ti_2GaN MAX phase compounds: First-principles study, *Heliyon,* **11** (2025) e42962. DOI: 10.1016/j.heliyon.2025.e42962

[33] M. Mebrek, A. Mokaddem, B. Doumi, A. Yakoubi, A. Mir, Novel theoretical prediction of structural properties, ferromagnetic ordering, and electronic structure of Fe_2PbC MAX phase, *Journal of Superconductivity and Magnetism*, **31** (2018) 2485–2490. DOI: https://doi.org/10.1007/s10948-017-4506-6

[34] M. Born, On the stability of crystal lattices. I, *Mathematical Proceedings of the Cambridge Philosophical Society,* **36** (1940) 160–172. DOI: https://doi.org/10.1017/S0305004100017138

[35] M. Born and R. Fürth, The stability of crystal lattices. III: An attempt to calculate the tensile strength of a cubic lattice by purely static considerations, *Mathematical Proceedings of the Cambridge Philosophical Society,* **36** (1940) 454-465. DOI: https://doi.org/10.1017/S0305004100017503

[36] S.-C. Wu, G.H. Fecher, S. Shahab Naghavi, C. Felser, Elastic properties and stability of Heusler compounds: Cubic Co_2YZ compounds with $L2_1$ structure, *Journal of Applied Physics,* **125** (2019*)* 082523. DOI: https://doi.org/10.1063/1.5054398

[37] Y. Tian, B. Xu, and Z. Zhao, Microscopic theory of hardness and design of novel superhard crystals, *The International Journal of Refractory Metals and Hard Materials,* **33** (2012*)* 93–106. DOI: https://doi.org/10.1016/j.ijrmhm.2012.02.021

[38] D.R. Lawati, H.K. Neupane, D.K. Chaudhary, P. Shrestha, R. P. Adhikari, L.P. Joshi, R. Parajuli, Structural, mechanical, electronic and optical properties of $MgZnO_3$ perovskite: First-principles study, *ornal of Physics and Chemistry of Solids,* **181** (2023) 111547. DOI: https://doi.org/10.1016/j.jpcs.2023.111547

[39] G.N. Greaves, A.L. Greer, R.S. Lakes, T. Rouxel, Poisson's ratio and modern materials, *Nature Materials.,* **10** (2011) 823–837. DOI: https://doi.org/10.1038/nmat3134

[40] J. Singh, *Optical Properties of Condensed Matter and Applications*, John Wiley & Sons, **6** (2006). DOI: 10.1002/0470021942

[41] H. Eshuis, J.E. Bates, F. Furche, Electron correlation methods based on the random phase approximation, *Theoretical Chemistry Accounts,* **131** (2012) 1084.

DOI: https://doi.org/10.1007/s00214-011-1084-8

[42] Y. Wu, X. Wang, Y. Wang, Y. Duan, M. Peng, Insights into electronic and optical properties of $AGdS_2$ (A = Li, Na, K, Rb and Cs) ternary gadolinium sulfides, *Optical Matererials,* **114** (2021) 110963. DOI: https://doi.org/10.1016/j.optmat.2021.110963

[43] C. Ambrosch-Draxl, J.O. Sofo, Linear optical properties of solids within the full-potential linearized augmented planewave method, *Computer Physics Communications,* **175** (2006) 1–14. DOI: https://doi.org/10.1016/j.cpc.2006.03.005

[44] B. Amin, I. Ahmad, M. Maqbool, S. Goumri-Said, R. Ahmad, *Ab initio* study of the bandgap engineering of $Al_{1-x}Ga_xN$ for optoelectronic applications, *Journal of Applied Physics,* **109** (2011) 023109. DOI: https://doi.org/10.1063/1.3531996

[45] M. Davies, Dielectric absorption, *Quarterly Reviews Chemical Society,* **8** (1954) 250. DOI: 10.1039/QR9540800250

[46] M.W. Qureshi, X. Ma, G. Tang, R. Paudel, *Ab initio* predictions of structure and physical properties of the Zr_2GaC and Hf_2GaC MAX phases under pressure, *Scientific Reports,* **11** (2021) 3260. DOI: https://doi.org/10.1038/s41598-021-82402-1

[47] B. Ul Haq, S.-H. Kim, S. AlFaify, M.A. Javed, R. Ahmed, K. Alam, A.R. Chaudhry, Physical properties of 211-type MAX phases based on Mn_2AlX (X = C, N, and F) through first-principles approaches, *Mater. Today Commun.,* **37** (2023) 107384. DOI: https://doi.org/10.1016/j.mtcomm.2023.107384

[48] M.A. Ali, M.T. Nasir, M.R. Khatun, A.K.M. A. Islam, S.H. Naqib, *Ab initio* investigation of vibrational, thermodynamic, and optical properties of Sc_2AlC MAX compound, *Chinese Physics B,* **25** (2016) 103102. DOI: 10.1088/1674-1056/25/10/103102

[49] H.K. Neupane, N.P. Adhikari, Structure, electronic and magnetic properties of 2D Graphene–Molybdenum diSulphide (G–MoS_2) heterostructure (HS) with vacancy defects at Mo sites, *Computational Condensed Matter,* **24** (2020) e00489. DOI: https://doi.org/10.1016/j.cocom.2020.e00489

[50] M.V. Makarova, Y. Akaishi, T. Ikarashi, K.S. Rao, S. Yoshimura, H. Saito, Alternating magnetic force microscopy: Effect of Si doping on the temporal performance degradation of amorphous FeCoB magnetic tips, *Journal of Magnetism and Magnetic Materials,* **471** (2019) 209–214. DOI: https://doi.org/10.1016/j.jmmm.2018.09.046

[51] M. Nepal, G. Paudel, S. Aryal, A. Devkota, H.K. Neupane, Adsorption of water on vacancy defective h-BN bilayer at B and N sites: First-principles calculation, *BIBECHANA,* **21** (2024) 129–141. DOI: https://doi.org/10.3126/bibechana.v21i2.62607

[52] G. Paudel, M. Nepal, S. Aryal, A. Devkota, H.K. Neupane, Effect of water adsorption on bilayer h-BN: First-principles study, *Journal of Nepal Physical Society,* **9** (2023) 56–62. DOI: https://doi.org/10.3126/jnphyssoc.v9i2.62323